Geoscientific
Model Development

Open Access

Methods to evaluate CaCO₃ cycle modules in coupled global biogeochemical ocean models

W. Koeve[1], O. Duteil[1], A. Oschlies[1], P. Kähler[1], and J. Segschneider[2]

[1]Biogeochemical Modelling, GEOMAR Helmholtz-Zentrum für Ozeanforschung, Düsternbrooker Weg 20, 24105 Kiel, Germany
[2]Max-Planck-Institut für Meteorologie, Bundesstraße 53, 20146 Hamburg, Germany

Correspondence to: W. Koeve (wkoeve@geomar.de)

Abstract. The marine CaCO₃ cycle is an important component of the oceanic carbon system and directly affects the cycling of natural and the uptake of anthropogenic carbon. In numerical models of the marine carbon cycle, the CaCO₃ cycle component is often evaluated against the observed distribution of alkalinity. Alkalinity varies in response to the formation and remineralization of CaCO₃ and organic matter. However, it also has a large conservative component, which may strongly be affected by a deficient representation of ocean physics (circulation, evaporation, and precipitation) in models. Here we apply a global ocean biogeochemical model run into preindustrial steady state featuring a number of idealized tracers, explicitly capturing the model's CaCO₃ dissolution, organic matter remineralization, and various preformed properties (alkalinity, oxygen, phosphate). We compare the suitability of a variety of measures related to the CaCO₃ cycle, including alkalinity (TA), potential alkalinity and TA*, the latter being a measure of the time-integrated imprint of CaCO₃ dissolution in the ocean. TA* can be diagnosed from any data set of TA, temperature, salinity, oxygen and phosphate. We demonstrate the sensitivity of total and potential alkalinity to the differences in model and ocean physics, which disqualifies them as accurate measures of biogeochemical processes. We show that an explicit treatment of preformed alkalinity (TA⁰) is necessary and possible. In our model simulations we implement explicit model tracers of TA⁰ and TA*. We find that the difference between modelled true TA* and diagnosed TA* was below 10 % (25 %) in 73 % (81 %) of the ocean's volume. In the Pacific (and Indian) Oceans the RMSE of A* is below 3 (4) mmol TA m⁻³, even when using a global rather than regional algorithms to estimate preformed alkalinity. Errors in the Atlantic Ocean are significantly larger and potential improvements of TA⁰ estimation are discussed. Applying the TA* approach to the output of three state-of-the-art ocean carbon cycle models, we demonstrate the advantage of explicitly taking preformed alkalinity into account for separating the effects of biogeochemical processes and circulation on the distribution of alkalinity. In particular, we suggest to use the TA* approach for CaCO₃ cycle model evaluation.

1 Introduction

According to Sabine et al. (2004), the ocean has taken up about 43 % of the anthropogenic CO₂ emissions into the atmosphere since preindustrial times. The partitioning of CO₂ between atmosphere and ocean is controlled by the buffer capacity of the CO₂-system in the surface ocean together with meridional overturning. The buffer capacity of the CO₂-system varies with temperature and the distribution of total inorganic carbon and alkalinity (e.g. Omta et al., 2010, 2011). Biogeochemical processes, namely the organic tissue pump and the CaCO₃ counter pump, strongly affect the ocean's internal cycling and distribution of carbon and alkalinity, which in turn influences the surface ocean buffer capacity and hence the ocean's ability to take up anthropogenic CO₂. Furthermore, the invasion of anthropogenic CO₂ into the ocean leads to ocean acidification, which is suspected to modify life conditions in the surface ocean potentially changing fluxes of carbon and alkalinity within the ocean. Potential feedbacks on the ocean's future capacity to take up anthropogenic CO₂

are likely to exist. To better understand and quantify possible global implications of CO$_2$-induced changes in ocean chemistry, numerical models of marine biogeochemistry and circulation are the method of choice. Data-based model evaluation is an important step in the development of prognostic models suitable for studying the complex interactions of ocean acidification, global warming, ocean biogeochemistry, and their net effect on global ocean carbon uptake and storage.

Considerable effort has been devoted to the evaluation of models of the organic tissue pump, i.e. the production, transformations, and fluxes of organic matter in the ocean. The distributions of nutrients (e.g. phosphate), oxygen, as well as derived properties like AOU, the apparent oxygen utilization (Pytkowicz, 1971), provide suitable constraints on organic matter fluxes in the ocean (Najjar et al., 2007; Schneider et al., 2008; Kriest et al., 2010; Duteil et al., 2013). These tracers are suitable because the effects of ocean biology on them has a large signal-to-background ratio, i.e. the biotic effect is large compared with other effects. For example, the ratio of phosphate remineralized in the interior of the ocean to total observed phosphate ranges between 20 and 45 % in high latitudes and oxygen minimum zones, respectively. This fraction can be even higher in shallow waters if preformed phosphate at the outcrop approaches zero. With AOU the signal-to-background ratio is even more favourable. Were it not for uncertainties in the oxygen saturation assumption required in its computation (Duteil et al., 2013) the effect of biota on AOU would be almost 100 %. The skill of state-of-the-art models to represent the organic tissue pump may hence be well judged from their ability to reproduce the global distribution of AOU (Najjar et al., 2007) or the recently suggested Evaluated Oxygen Utilization (EOU, Duteil et al., 2013).

In contrast, evaluating models of the marine CaCO$_3$ cycle is more difficult. Total alkalinity (TA) has frequently been used for this purpose. However, patterns of TA reflect not only the production and dissolution of CaCO$_3$. In this study we look for adequate tracers which are suited to evaluate the marine CaCO$_3$ cycle in biogeochemical models. In Sect. 2 we show that surface ocean patterns of TA are dominated by evaporation and precipitation. Using observations as well as model results we discuss these and other limitations of TA for model evaluation. In Sect. 3 we introduce an approach which has been proposed to explicitly account for non-CaCO$_3$ effects on TA, the TA* concept (e.g. Feely et al., 2002). TA* measures the time-integrated imprint of CaCO$_3$-dissolution in the ocean. It is an analogue of AOU, which measures time-integrated oxygen utilization. In Sect. 4 we present our experimental approach to test the applicability of TA* by means of model simulations, in which computed TA* is compared with an explicit, idealized, TA* model tracer. In Sect. 5 we present and discuss the results of the assessment of TA*. Finally (Sect. 6), we apply the TA* approach to real-ocean observations as well as several published models. Note that in this study we assess the suitability of different methods to evaluate modules of the CaCO$_3$ cycle. Applying these methods to evaluate actual state-of-the-art models, e.g. CMIP5, will be the subject of a future study.

2 TA distribution and CaCO$_3$ transformations

The production and dissolution of CaCO$_3$ affect the concentrations of calcium, total dissolved inorganic carbon (TCO$_2$), and total alkalinity (TA). However, it is only TA and TCO$_2$ for which the total number of observations and their distribution (GLODAP, Key et al., 2004) can support model evaluation on a global scale. The sensitivity of TCO$_2$ to production and dissolution of CaCO$_3$ is very low since TCO$_2$ is predominately modified by decay of organic matter and influenced by the invasion of anthropogenic CO$_2$. In 99 % of the ocean interior, organic matter decay has a larger effect on TCO$_2$ than CaCO$_3$ dissolution (Fig. 1a). The property (TA-TCO$_2$) has recently been employed to assess a model's potential to take up atmospheric CO$_2$ (Séférian et al., 2013; Dunne et al., 2013). This is motivated by the fact that (TA-TCO$_2$) serves as a good approximation for the carbonate ion concentration at the surface which itself is inversely related to the chemical capacity of the ocean to take up CO$_2$ from the atmosphere (Sarmiento and Gruber, 2006; Séférian et al., 2013). In the interior of the ocean (TA-TCO$_2$) is modified by both the remineralization of organic matter and the dissolution of CaCO$_3$. In the deep ocean (GLODAP data, not shown) the impact of organic matter remineralization strongly dominates the patterns of (TA-TCO$_2$). On the 2000 m depth plane, for example, 92 % of the variance of (TA-TCO$_2$) is explained by variations of AOU. The property (TA-TCO$_2$) is hence not suitable to assess a model's CaCO$_3$ cycle.

The effect of CaCO$_3$ dissolution on TA exceeds that of organic matter remineralization in about 60 % of the ocean volume (Fig. 1b) making TA more appropriate to evaluate CaCO$_3$ models. Therefore TA is often used as a data constraint in global CaCO$_3$ modelling (e.g. Gehlen et al., 2007; Ilyina et al., 2009; Ridgwell et al., 2007). A major concern, however, in using TA concentrations for data-based model evaluation is the fact that it has a large background. In the deep North Pacific Ocean, where the largest time-integrated imprint of CaCO$_3$ dissolution is observed (about 120 mmol TA m^{-3}, Feely et al., 2002), it is equivalent to 5 % of the observed TA only. Everywhere else the contribution of CaCO$_3$ dissolution on TA is even lower. On a global average, the ratio of the CaCO$_3$-dissolution imprint to TA-background is about 0.02. The global mean ratio of the alkalinity effect stemming from organic matter remineralization to TA background is only 0.005. Contributions from N$_2$-fixation, denitrification, sulfate reduction, and shelf alkalinity fluxes are even smaller or of local importance only. Due to the dominance of the TA background, TA behaves to a large extent like a conservative tracer, very much like salinity. In fact about 71 % of the variation of surface ocean alkalinity of the
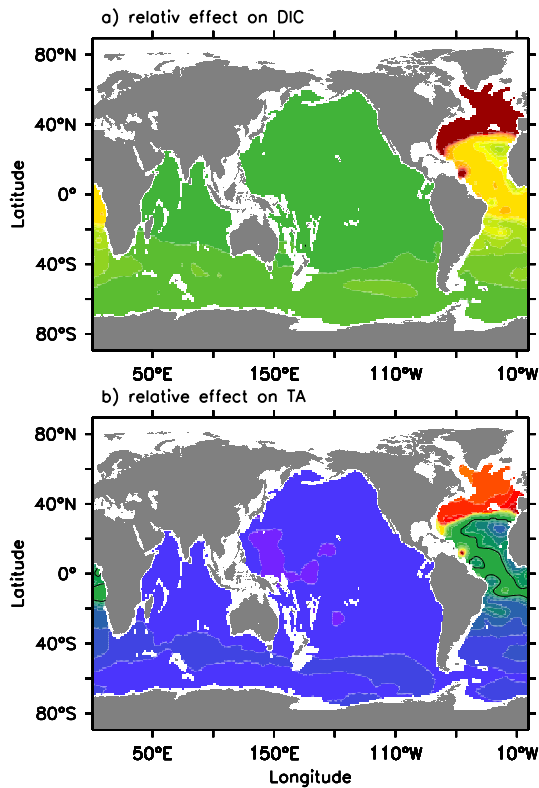
Figure 1. Ratio of the imprint of the organic tissue pump and the CaCO$_3$ pump on TCO$_2$ (**a**) and TA (**b**) at 2000 m water depth. ΔDIC$^{\text{tissue}}$ and ΔTA$^{\text{tissue}}$ are computed from estimates of the apparent oxygen utilization (AOU) and the mean molar oxygen : carbon ratio of 1.4 and the mean molar oxygen : alkalinity ratio of 0.119 ($= 1/170 \times 16 \times 1.26$), respectively. AOU is estimated using oxygen, potential temperature and salinity data from the World Ocean Atlas (gridded data, analysed annual means). ΔTA$^{\text{CaCO}_3}$ is computed using the TA* method described in Sect. 3 applied to the GLODAP gridded data set (Key et al., 2004). ΔDIC$^{\text{CaCO}_3} = 0.5 \times$ TA*.

Figure 2. Surface ocean distribution of TA (**a**, GLODAP, gridded data, http://cdiac.ornl.gov/ftp/oceans/GLODAP_Gridded_Data/, last access: 10 December 2009) and salinity (**b**, World Ocean Atlas, WOA, analysed annual means, Antonov et al., 2010). The scaling of the isolines was chosen to emphasize the global linear relationship between alkalinity (μmol kg^{-1}) and salinity. With ungridded bottle data from the upper 100 m of the ocean (GLODAP/WAVES data set, http://cdiac3.ornl.gov/waves/discrete/, last access: 31 March 2012) this relationship is TA $= 699.75 + 46.18 \cdot S$; $r^2 = 0.71$.

GLODAP data composite is explained by salinity variation (Fig. 2). This is easily understood since alkalinity represents the charge balance of the major constituents of sea salt, and like salinity, surface ocean alkalinity is largely determined by evaporation and precipitation (e.g. Friis et al., 2003). In the ocean interior its distribution is largely explained by advection and mixing of "preformed alkalinity" (Fig. 3a and b). In analogy to the concept of preformed nutrients or preformed oxygen (Redfield et al., 1963; Duteil et al., 2012, 2013), preformed alkalinity (in the following denoted TA^0) refers to the alkalinity which a water mass had when last in contact with the atmosphere before being subducted (Chen and Millero, 1979). In the ocean interior TA^0 is a strictly conservative tracer, whereas TA is variable due to transformations of CaCO$_3$ and organic matter. These principles apply both to models and the real ocean, yet there is the difficulty that in the real ocean TA^0 cannot be separated from TA by
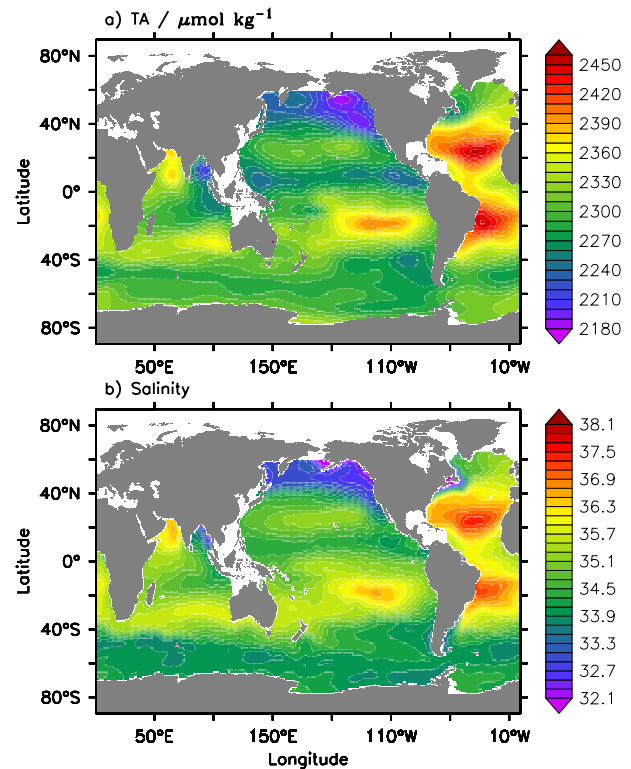
measurements. In a model, the distribution of TA^0 can be studied by designing an explicit tracer of TA^0 (see Sect. 4 for details). Along a section at 30° W in the Atlantic (Fig. 4), the range of modelled TA^0 values is equivalent to 97 % of the range of modelled TA; along a section at 150° W in the Pacific (not shown) the respective value is 69 % in our model (see Sect. 4 for a description of the model). Given that physical processes can never be represented perfectly in coupled biogeochemical circulation models (e.g. Doney et al., 2004), it is not recommended to use the distribution of bulk TA as a descriptor of CaCO$_3$ transformations in a data–model comparison. Small deficiencies in the representation of TA^0, e.g. due to errors in the surface salinity balance, or errors in ocean circulation and mixing, can have profound effect on TA distribution in the ocean interior. Apparently good (Fig. 5a) or bad (Fig. 5c and d) fits of model and observed TA (Fig. 5b) may hence betray our judgement of the respective CaCO$_3$ modules.
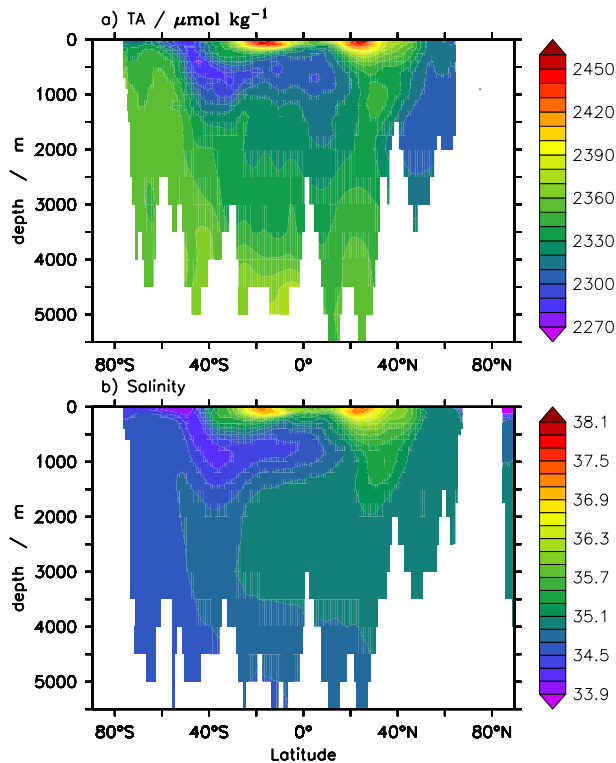
Figure 3. Horizontal sections of alkalinity (**a**, GLODAP) and salinity (**b**, WOA) along 30° W in the Atlantic Ocean. For the scaling of the isolines see caption of Fig. 2. Alkalinity patterns, particularly in the upper 2000 m, largely follow patters of salinity indicating a predominantly conservative behaviour of alkalinity in the interior of the Atlantic Ocean. The r^2 of (**a**) over (**b**) is 0.692.

Figure 4. Distribution of total alkalinity (**a**) and a preformed alkalinity tracer (**b**) along 30° W from a model run (TMM-MIT28, see Sect. 4 for details of the model experiments). The r^2 of (**a**) over (**b**) is 0.631. The preformed alkalinity (TA^0) tracer is restored at the surface and at any time step of the model run to total alkalinity. In the interior of the model ocean TA^0 has no biogeochemical sources or sinks but is advected and mixed conservatively. TA in this model is affected by both physical and biogeochemical processes.

Recognizing these shortcomings of using TA patterns to estimate CaCO$_3$ cycling, different approaches have been proposed to overcome them. For example, Howard et al. (2006), suggested a tracer Alk* = Alk − Alk^{mean}/S^{mean} · S, with Alk^{mean} and S^{mean} being the oceanwide means of alkalinity and salinity, respectively. Variation of this Alk* tracer in the deep ocean is supposed to be driven by CaCO$_3$ dissolution (increase in alkalinity) and the remineralization of organic matter (decrease in alkalinity) only (Howard et al., 2006). (For the purpose of not confusing Howard's Alk* tracer with other tracers we use in our study, we rename their Alk* as TA^{H06} = TA − TA$_{ave}$/S_{ave} · S.) The emerging pattern of this tracer along a transect in the Atlantic (Fig. 6a) suggests a dominance of CaCO$_3$ production (and/or organic matter remineralization) in the North Atlantic and of CaCO$_3$ dissolution in waters originating from the Southern Ocean. Applying Howard's approach to our model tracer TA^0, we compute the anomaly TA^0 − TA$^0_{ave}$/S_{ave} · S. As the TA^0 tracer behaves conservatively within the ocean, its anomaly should not reflect any local effects of either CaCO$_3$ dissolution or organic matter remineralization. However, the patterns of this anomaly in our model simulation (Fig. 6b) are very similar to the pattern of the Howard et al. (2006) tracer (Fig. 6a) itself,
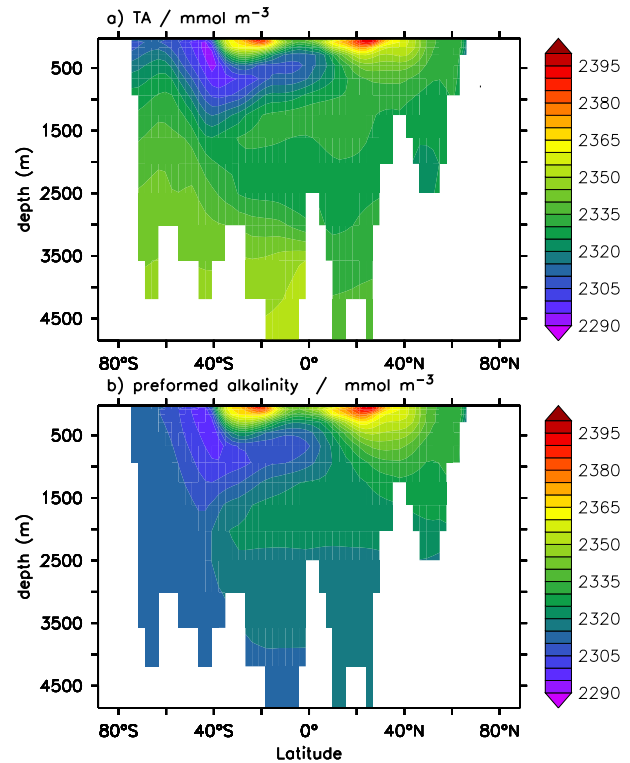
indicating that the Howard et al. (2006) tracer is not informative about where and how much CaCO$_3$ dissolves.

Another property suggested as a tracer of CaCO$_3$ transformations, which excludes any effects of salinity and organic tissue production or remineralization, is Potential Alkalinity (PALK = (TA + NO$_3$)/S · 35, e.g. Sarmiento et al., 2002). Here, the salinity normalization is to correct for the effects of the freshwater balance and the nitrate term is to compensate for the alkalinity effects of organic matter dynamics. Yet again, modelled patterns of both PALK and PALK^0 = (TA^0 + PO$_4^0$ · 16)/S · 35) in the Atlantic (Fig. 6c, d) trace characteristic water masses observed in the Atlantic Ocean, like North Atlantic Deep Water, Antarctic Intermediate Water and Antarctic Bottom Water conservatively. Patterns of PALK can hence not straightforwardly be interpreted in terms of the local process of CaCO$_3$ dissolution or production.

In the real ocean, simple salinity normalization like in the TA^{H06} or PALK metrics cannot remove water mass effects since they are due to a variety of processes. For example, there is the effect of non-zero alkalinity freshwater sources
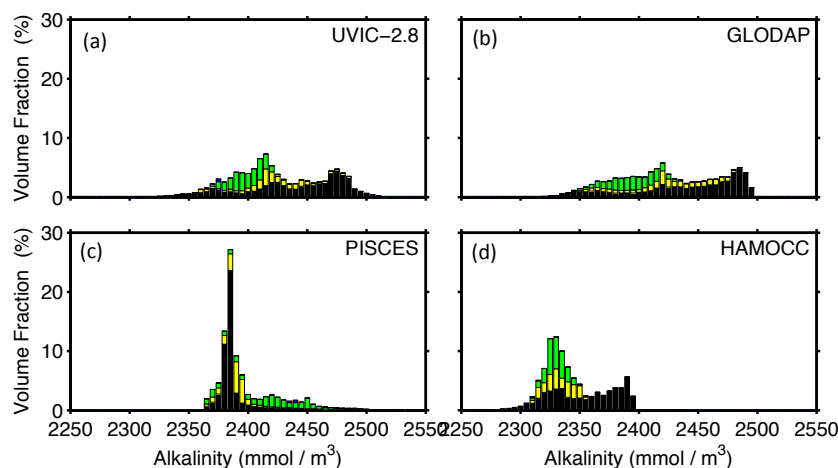
Figure 5. Global ocean volume-weighted frequency-distribution of alkalinity in observations (GLODAP data set, Key et al., 2004) and three global carbon cycle models (see Duteil et al., 2012 for details). Fractions of the Atlantic, Pacific, Indian and Arctic Oceans are indicated by colour codes (green, black, yellow and blue, respectively).

(Robbins, 2001; Friis et al., 2003), which are highly variable on a global scale. In the Atlantic, for example, riverine zero-salinity alkalinity ranges from about 250 (Amazon) to 2500 (Mississippi) mmol m^{-3} (e.g. Cai et al., 2010). Freshwater alkalinity depends on geochemical conditions of the respective drainage basins. In models, zero-salinity alkalinity end members depend on model-specific alkalinity ocean-boundary conditions. However, neither of these effects can explain the distribution of PALK and PALK^0 in the ocean's interior of our model simulation. Here, two additional problems of the PALK concept become obvious: the biogenic modifications of TA in the surface ocean and, in particular, the recirculation of TA in the Southern Ocean. CaCO₃ production in the surface ocean changes TA and consequently affects TA^0. The PALK concept does not correct for this effect and hence the imprint of surface CaCO₃ production travels with PALK and PALK^0 through the interior of the ocean where, being subject to mixing, it complicates the interpretation of PALK with respect to CaCO₃ dissolution. Concerning the PALK (and TA^{H06}) patterns in the South Atlantic (Fig. 6), however, the recirculation of TA is likely to be most important. The Southern Ocean is the major site where deep water returns to the surface (Marshall and Speer, 2002). Water which has accumulated the imprint of CaCO₃ dissolution in the North Pacific returns to the surface in the Southern Ocean. Subsequently, most of this water is re-injected into the interior of the ocean either as Antarctic Intermediate Water or Antarctic Bottom Water. Similarly, the imprint of oxygen utilization in the ocean's interior wells up in the Southern Ocean, indicated by significant oxygen undersaturation there (Ito et al., 2004). Gas exchange with the atmosphere, however, is able to reset oxygen to values corresponding to surface temperature and salinity nearly completely. But for TA no equivalent restoring process to reset it to values consistent

with actual surface salinity exists. The PALK pattern observed in the South Atlantic must hence be interpreted as a recirculation of the imprint of CaCO₃ dissolution having taken place as far away as the North Pacific. We conclude that neither TA data nor derivatives like TA^{H06} or PALK are well suited for the data-based evaluation of ocean CaCO₃ cycle models. Computing the difference between PALK and PALK^0 (Anonymous, 2013) leads us to a property which has been used for the quantification of CaCO₃ dissolution. Ignoring the effect of denitrification and assuming N / P and O₂ / P ratios of 16 and 170, this difference can be rewritten as (TA − TA^0 + NO₃ − NO$_3^0$)/S·35 =(TA − TA^0 + NO₃remin)/S·35. In this way the imprint of CaCO₃ dissolution would be computed from observed TA, an explicit estimate of preformed TA, and an estimate of the alkalinity effect of organic matter remineralization. In the next section we describe TA*, a similar property, suggested earlier as a measure of the time-integrated effect of CaCO₃ dissolution in the ocean (Feely et al., 2002; Sabine et al., 2002; Chung et al., 2003).

3 TA* approach

The TA* approach (Feely et al., 2002; Sabine et al., 2002; Chung et al., 2003) has been used to quantify the time-integrated imprint of CaCO₃ dissolution. Variants of this method have been vital for the determination of anthropogenic CO₂ in the ocean since the early paper of Chen and Millero (1979). The underlying concept (Eq. 1) of the TA* approach is that the observed alkalinity (TA) in the interior of the ocean is composed of a preformed component, TA^0, a term caused by the remineralization of organic matter, TA^r, and a term due to CaCO₃ dissolution, usually coined TA* (unlike in other publications, and for the sake of the direct comparison of computed TA* and the TA* tracer introduced
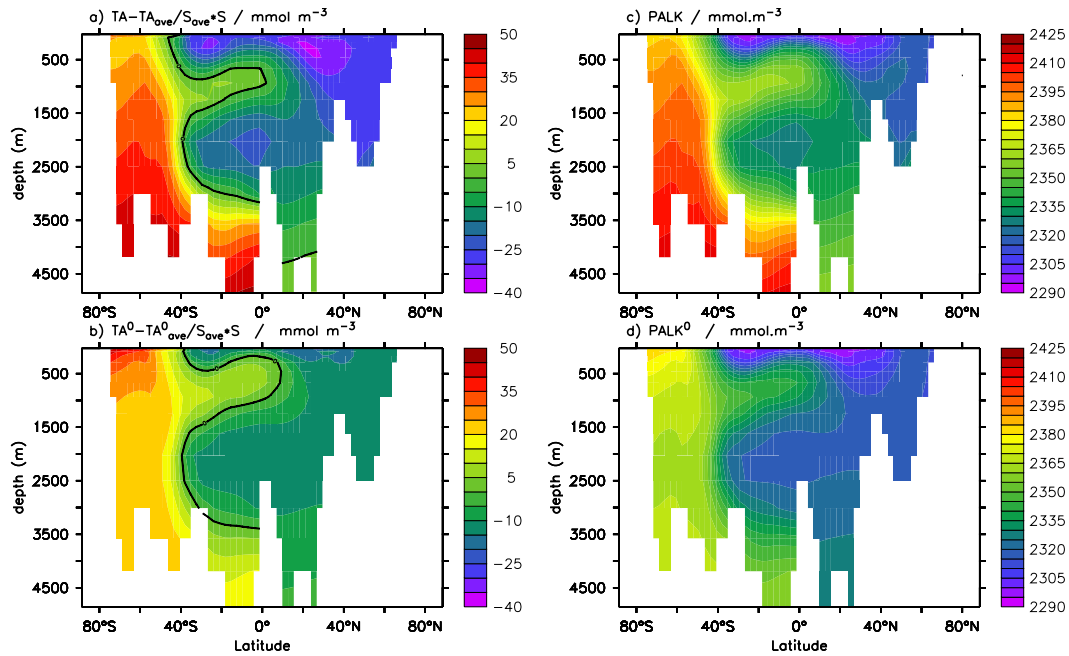
Figure 6. Anomalies of TA (**a**) and TA^0 (**b**) and the respective salinity normalized properties. (**c**) Potential alkalinity $PALK = (ALK + PO_4 \cdot 16)/S \cdot 35$ distribution along a section through the Atlantic. (**d**) Potential preformed alkalinity $PALK^0 = (TA^0 + PO_4^0 \cdot 16)/S \cdot 35$. The distribution along 30° W from a model run (TMM-MIT28, see Sect. 4 for details of the model experiments) is shown.

below, all terms are in units of mmol TA m⁻³):

$$TA = TA^0 + TA^* - TA^r. \tag{1}$$

Remineralization of organic matter, through the regeneration of nitrate, phosphate and sulfate, decrements TA while the dissolution of $CaCO_3$ increments it (Wolf-Gladrow et al., 2007). The alkalinity effect of organic matter decomposition can be parametrized as a function of AOU, i.e. $TA^r = r_{Alk:NO_3} \cdot r_{NO_3:-O_2} \cdot AOU$. Values for $r_{NO_3:-O_2}$ and $r_{Alk:NO_3}$ are usually derived from observations, e.g. $r_{NO_3:-O_2} = 1/10.625$, $r_{Alk:NO_3} = 1.26$ (Anderson and Sarmiento, 1994; Kanamori and Ikegami, 1982), and are generally prescribed in biogeochemical models. Considering maximum values of AOU observed in the ocean (about 350 mmol O_2 m⁻³), the largest TA^r is about 40 mmol TA m⁻³. The global average TA^r (using AOU from the World Ocean Atlas) is 18.1 mmol m⁻³. Considering AOU to overestimate true oxygen utilization by 20–25 % (Ito et al., 2004; Duteil et al., 2013), TA^r computed from AOU is probably also overestimated accordingly.

Preformed alkalinity denotes the alkalinity, which a water parcel had during its last contact with the atmosphere (Chen and Millero, 1979). Since all water masses in the interior of the ocean are mixtures of various end-members, the preformed alkalinity is also a mixture of different end-member alkalinity concentrations. For a given location in the ocean interior, neither the preformed alkalinity end-member concentrations nor their mixing ratios are known. Preformed

alkalinity, TA^0, must therefore be diagnosed. This is usually done by an empirical approach which comprises two steps (e.g. Feely et al., 2002; Matsumoto and Gruber, 2005. First, a multi-linear regression of alkalinity with salinity, temperature and PO (or NO) is derived from near-surface data:

$$TA^{surf} = a_0 + a_1 \cdot S^{surf} + a_2 \cdot T^{surf} + a_3 \cdot PO^{surf}. \tag{2}$$

PO (or NO) are considered conservative tracers within the ocean (Broecker, 1974) and defined as $PO = O_2 + r_{-O_2:PO_4} \cdot PO_4$, and $NO = O_2 + r_{-O_2:NO_3} \cdot NO_3$, assuming that $r_{-O_2:PO_4}$ and $r_{-O_2:NO_3}$ are constant in the interior of the ocean ($r_{-O_2:PO_4} = 170$; $r_{-O_2:NO_3} = 10.625$; Anderson and Sarmiento, 1994). Secondly, the coefficients derived from surface data are subsequently applied to salinity, potential temperature and PO (or NO) data from the interior of the ocean to compute TA^0 everywhere:

$$TA^0(x, y, z) = a_0 + a_1 \cdot S(x, y, z) \\ + a_2 \cdot potT(x, y, z) + a_3 \cdot PO(x, y, z). \tag{3}$$

We will here use salinity, temperature and PO from the upper 100 m to derive the regression coefficients of Eq. (2). Salinity normalization of alkalinity has been applied sometimes with the TA^* approach, but it is omitted here following Friis et al. (2003) and the results presented in Sect. 2. Given these estimates of TA^0 and TA^r and observations or model tracer data of TA, TA^* can be computed after rearranging Eq. (1). In the following we will refer to this explicit way to quantify TA^* (i.e. Eqs. 1–3) as the "TA^* method".

4 Modelling approach

Although variants of the TA* method have been in use for decades there has, to our knowledge, not been any explicit and quantitative assessment of this method. The main reason for this is that in the real ocean no independent and rigorous approach to quantify the imprint of CaCO$_3$-dissolution exists. Hence the potential and limitations of the TA*-method have never been tested. Here, we apply a prognostic global ocean carbon cycle model for this purpose. The model consists of an offline representation of ocean physics providing transport and mixing within the ocean, a NPZD-type model to represent the organic tissue pump, a CaCO$_3$ cycle module, as well as idealized tracers of TA^0, TA* and TA^r.

For the physical model we use the transport matrix method (TMM) described in detail by Khatiwala et al. (2005) and Khatiwala (2007). In this approach, passive tracer transport is represented by a matrix operation involving the tracer field and a transport matrix extracted from the MIT general circulation model, a primitive equation ocean model (Marshall et al., 1997). Seasonally cycling (monthly) coarse-resolution matrices were derived from a $2.8° \times 2.8°$ global configuration of this model with 15 layers in the vertical, forced with monthly mean climatological fluxes of momentum, heat and freshwater, and subject to a weak restoring of surface temperature and salinity to observations. The same transport matrices were employed by Kriest et al. (2012) in their data-based assessment of biogeochemical models.

The model of the organic tissue pump used with the TMM is the NPZD–O$_2$–DOP model of Schmittner et al. (2005) as modified by Kriest et al. (2010, 2012). The primary model currency is phosphorus (phosphate, DOP, phytoplankton, zooplankton, detritus) with oxygen as an additional model tracer. The molar O$_2$: P ratio is fixed at 170 (Anderson and Sarmiento, 1994). Sinking and remineralization of detritus are parametrized by a combination of a constant remineralization rate and particle sinking speeds increasing with depth, together reflecting a power-law function of the flux profile (Martin et al., 1987) with an exponent of 1.075 (Kriest et al., 2010). The latter value has been found to yield global oxygen and phosphate distributions in good agreement with observations (Kriest et al., 2012).

In order to represent oceanic alkalinity in a pragmatic way we implement the tracer TA and couple the production and remineralization of organic matter with fixed ratios to the uptake and release of phosphate in the NPZD–O$_2$–DOP model. We use a TA : P ratio of 21.8. CaCO$_3$ is produced with a temperature-dependent inorganic carbon : organic carbon ratio bound to the rate of detritus production in the model. The global CaCO$_3$ export production of our model is 0.9 Gt C year^{-1}, similar to other models and observational estimates (Berelson et al., 2007). In our model, CaCO$_3$ export and dissolution are instantaneous and follow an exponential decay function with a decay length scale of 2000 m. Although this may not be a mechanistic representation of the processes involved in CaCO$_3$ dissolution, it is a pragmatic parametrization. It has previously been used e.g. in the UVIC model (see Sect. 6 below for a brief description of the models employed), which yield TA-distributions (Fig. 5) and TA* global mean profiles (Sect. 6) in good agreement with observations. We present preindustrial Holocene steady-state results from a model run over 6000 years of model integration.

4.1 Idealized tracers

We implement a number of idealized tracers. The tracer of preformed alkalinity, TA^0, is restored to model TA everywhere at the surface and at every time step. In the interior of the model ocean this tracer has no sinks or sources, but is transported and mixed conservatively according to our model's physics. The TA* tracer is set to zero at the surface. In the interior of the model ocean this tracer collects the effect of CaCO$_3$ dissolution whenever it occurs. Similarly, a TA^r tracer is set to zero at the surface and collects the alkalinity effect of organic matter remineralization in the ocean interior. All idealized tracers are transported and mixed according to model physics. In this way, we perfectly know TA^0, TA* and TA^r at any point and time in the model. It is run for 6000 years until practically at each grid point the sum of the idealized tracers equals the model's TA, i.e. Eq. (1) is satisfied. In order to test the TA* concept we compare the model tracers TA^0 and TA* (in the following denoted TA$^0_{\text{true}}$ and TA$^*_{\text{true}}$) with these two properties as diagnosed from the model TA, PO$_4$, T, S, O$_2$, and AOU, according to Eqs. (1)–(3). In the following the diagnosed properties are denoted TA$^0_{\text{diag}}$ and TA$^*_{\text{diag}}$, respectively.

4.2 TA^0 algorithms

The initial step in the TA* approach is to derive a multi-linear relationship between alkalinity and temperature, salinity and PO in the surface ocean (see Eq. 2). In the past, TA* has been computed from observations using algorithms based on either global data sets (e.g. Matsumoto and Gruber, 2005) or basin-wide subsets (Feely et al., 2002; Sabine et al., 2002; Chung et al., 2003), depending on the scope of the respective studies. Here, we test whether more regionally based algorithms will provide improved estimates of TA^0 and eventually TA* for data from our model experiment. Another limitation of TA^0 algorithms derived from observations may be a seasonal bias in high-latitude observations of alkalinity (and many other surface ocean properties). Water masses present in the deep ocean usually form in high-latitude outcrop regions at the end of winter, a season when ship-based field studies are difficult. Ship-based data from winter in high latitudes are therefore scarce (e.g. Koeve, 2006) and sampling is biased toward spring, summer and autumn. This seasonal bias may pose a problem since the data used to derive a multi-linear regression with surface alkalinity, namely sea surface temperature and surface

ocean PO do not behave conservatively over the seasonal cycle. Temperatures are higher in summer than in winter and, because of temperature-induced outgassing of oxygen, PO is lower in summer. It may therefore be speculated that TA^0 algorithms derived from seasonally biased surface data do not predict interior ocean TA^0 reliably. We test this by deriving algorithms based on sampling the surface ocean of our model either seasonally unbiased, summer biased or winter biased. The expectation is that winter-biased TA^0 algorithms should provide the best predictions of TA*. In order to derive the seasonally unbiased TA^0 algorithms we sample monthly resolved model output during every month and at every grid box at the surface. For the seasonally biased sampling, we use the same model output but sampled only during the given season of the respective hemisphere. We defined winter as January–March (July–September) in the Northern (Southern) Hemisphere.

5   TA* method assessment

In the following we compare the model's true TA* (TA$^*_{\text{true}}$ being the TA* tracer) with TA$^*_{\text{diag}}$ estimated from the model output (according to Eqs. 1 to 3). Using TA$^*_{\text{true}}$ as a reference we compute volume weighted RMSEs of TA$^*_{\text{diag}}$ aggregated on global and basin scales and for different depth levels, i.e.

$$\text{RMSE} = \sqrt{\left[\sum_{i,j,k}\left(\text{vol}_{i,j,k}/\text{vol}_{\text{total}} \times \left(\text{TA}^*_{\text{diag}} - \text{TA}^*_{\text{true}}\right)^2_{i,j,k}\right)\right]}. \quad (4)$$

We apply this approach to different sets of diagnosed TA* which are distinguished by the different seasonally biased estimates of TA^0 (see previous section). In order to isolate the error related to the computation of TA^0 we here ignore any error related to the estimation of TA^r from diagnosing AOU and use the explicit model tracer of TA^r when computing TA*, i.e. TA$^*_{\text{diag}} = \text{TA} - \text{TA}^0_{\text{diag}} + \text{TA}^r_{\text{true}}$.

Using a single global algorithm (Table 1, #1) derived from the seasonally unbiased sampling of surface ocean data for the computation of preformed alkalinity (TA$^0_{\text{ub}}$), we can reproduce the TA$^*_{\text{true}}$ distribution relatively well: the global average volume-weighted RMSE of TA* in the interior of the ocean (below 100 m) is 5.8 mmol m^{-3} (Table 2, #1) and the global mean profiles of TA$^*_{\text{diag}}$ and TA$^*_{\text{true}}$ show very similar vertical patterns, while TA$^*_{\text{diag}}$ is generally somewhat smaller than TA$^*_{\text{true}}$ (Fig. 7a). The performance of the global algorithm varies with ocean basin, with RMSEs as low as 2.8 mmol m^{-3} and as high as 10.4 mmol m^{-3} in the Pacific and Atlantic oceans, respectively (Table 2). Using TA^0 algorithms derived from regional data reduces the RMSE slightly in the Atlantic and Indian Oceans, while increasing it in the Pacific Ocean. The surface alkalinity RMSE (column 2 in Table 2) has little predictive power for the RMSE of TA*
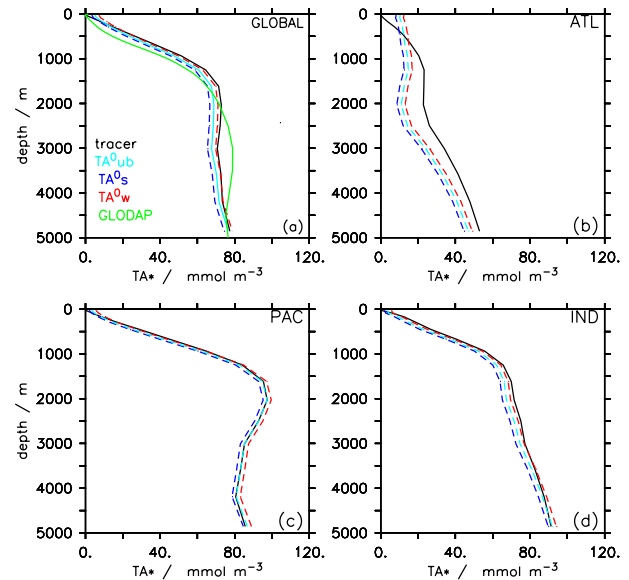

Figure 7. (a) Global mean profile of TA* from explicit model tracer (black, solid) and computed from model data (dashed). The two dashed lines are based on seasonally biased sampling of the model output at the surface when deriving the TA^0 algorithm. TA^0_s refers to sampling during summer, TA^0_w refers to winter sampling when deep water actually forms. TA$^0_{\text{ub}}$ refers to seasonally unbiased sampling. For comparison, the green line shows the global mean profile of TA* computed from the GLODAP database and using a globally uniform algorithm derived from the gridded surface GLODAP data **(b–d)**. Basin-averaged profiles of TA* for the Atlantic, Pacific and Indian oceans. Tracer-based estimate (black, solid) and computed TA* from winter- and summer-biased TA^0 algorithms are shown.

in the interior of the ocean. Basin-averaged vertical profiles (Fig. 7b–d), show excellent agreement of diagnosed and true TA* in the Pacific while in the Atlantic, TA$^*_{\text{diag}}$ is an underestimate of TA$^*_{\text{true}}$. Basin-averaged vertical profiles of the TA* RMSE (Fig. 8a) are rather uniform in the Pacific and Indian oceans and have subsurface maxima at 2000 m depth in the Atlantic Ocean. The basin-average relative error of TA* is 10 % or less in the Pacific and Indian oceans below about 1000 m water depth (Fig. 8c). In the Atlantic Ocean the relative error (TA$^*_{\text{RMS}}$/TA* · 100) is higher throughout and above 30 % in most of the water column, because of large RMSEs and low TA* signal strength (Fig. 8b).

Using seasonally biased surface data to derive the TA^0 algorithms yields increased TA* RMSEs for summer-biased sampling and usually slightly reduced TA* RMSEs for winter-biased sampling (Table 3). However, the effects of seasonally biased surface sampling are modest. Again, RMSEs of surface alkalinity have little predictive power for TA* RMSEs. Using regional surface data to derive the TA^0 algorithm improves the TA* computation in some cases, like in the Indian or in the Pacific Oceans during summer (Table 2). However, using only surface Atlantic Ocean data to derive the TA^0 algorithm does not solve the problem of high

Table 1. TA^0 algorithms. Algorithms are derived from surface data (upper 100 m) of the model. Subsets "winter data" "summer data") use surface data from winter (summer) months of the respective hemispheres only. Basin-specific algorithms are based on data from the respective ocean basin.

#	Subset	Equation
	Global	
1	All months	$TA^0 = 370.5765 + 54.0812 \cdot S + 0.3804 \cdot T + 0.1129 \cdot PO$
2	Winter data	$TA^0 = 357.9100 + 54.3812 \cdot S + 0.3824 \cdot T + 0.1130 \cdot PO$
3	Summer data	$TA^0 = 336.2851 + 55.0656 \cdot S + 0.4047 \cdot T + 0.1167 \cdot PO$
	Atlantic	
4	All months	$TA^0 = 263.3001 + 56.1655 \cdot S + 1.4997 \cdot T + 0.1702 \cdot PO$
5	Winter data	$TA^0 = 122.0885 + 59.9151 \cdot S + 1.5293 \cdot T + 0.1857 \cdot PO$
6	Summer data	$TA^0 = 323.8251 + 54.4048 \cdot S + 1.6823 \cdot T + 0.1737 \cdot PO$
	Pacific	
7	All months	$TA^0 = 559.3595 + 49.0273 \cdot S + 0.0923 \cdot T + 0.0861 \cdot PO$
8	Winter data	$TA^0 = 550.7772 + 49.3419 \cdot S - 0.0299 \cdot T + 0.0794 \cdot PO$
9	Summer data	$TA^0 = 506.9215 + 50.5235 \cdot S + 0.1332 \cdot T + 0.0903 \cdot PO$
	Indic	
10	All months	$TA^0 = 844.9869 + 40.6930 \cdot S + 0.0261 \cdot T + 0.0960 \cdot PO$
11	Winter data	$TA^0 = 715.8663 + 44.1346 \cdot S + 0.2181 \cdot T + 0.1095 \cdot PO$
12	Summer data	$TA^0 = 824.6536 + 41.4498 \cdot S - 0.1242 \cdot T + 0.0902 \cdot PO$

Table 2. Volume-weighted RMSEs of global and regional TA^0 and TA^* estimates. Errors given in column "Surface" refer to the ability of the respective algorithm to reproduce the surface (upper 100 m) alkalinity of the model. Under TA^0 RMSEs of subsurface preformed TA as compared with TA^0 from the explicit tracer are given. Under TA^* RMSEs of computed TA^* compared with TA^* from the explicit tracer are given. Global algorithms are also evaluated concerning their skill on regional scales.

Algorithm	Surface	Global		Atlantic Ocean		Pacific Ocean		Indian Ocean	
		TA^0	TA^*	TA^0	TA^*	TA^0	TA^*	TA^0	TA^*
Global	9.6	6.5	5.9	10.2	10.4	4.3	2.8	4.4	3.8
Atlantic	9.7			10.3	10.1				
Pacific	9.2					3.1	3.5		
Indic	5.9							3.2	2.7

TA^* RMSEs there. It is worth noting that despite the large RMSEs, diagnosed TA^0 still resembles the overall regional patterns of true TA^0 in the interior of the Atlantic Ocean (Fig. 9). We speculate that this is caused by the complex mixture of waters subducted in the north and south with their different end-member properties. Neither the global nor the basin-scale TA^0 algorithm can predict TA^0 in the interior of the Atlantic Ocean well enough to allow reasonable TA^* estimates. This is also reflected by particularly large RMSEs of the TA^0 estimate in the North Atlantic Deep Water (NADW) (Fig. 9d), where the TA^0 algorithm overestimates TA^0 by 10–14 mmol m^{-3} (Fig. 9c).

Zonal averages of TA^*_{true} in the Pacific and Atlantic oceans are compared with the difference of diagnosed and true TA^* (Fig. 10). In intermediate waters of the Atlantic, but also in

the North Atlantic Deep Water, uncertainties of TA^* are of similar magnitude as TA^*. It is only in Antarctic Bottom Water that uncertainties are small enough to detect TA^* in the Atlantic. In the Pacific the picture is quite different. TA^* is detectable almost everywhere except in surface and mode waters of the upper several hundreds of metres.

As a note of caution it is stressed again that TA^* is a time-integrated property subject to advection and mixing. The occurrence of a large TA^* values at a given location does not necessarily indicate the rate of CaCO₃ dissolution to be particularly large there. This characteristic of TA^* is shared with many other cumulative properties, notably AOU, which represents the time-integrated measure of remineralization of organic matter, not its actual, local rate. The observation of TA^* in shallow waters oversaturated with respect to the dominant
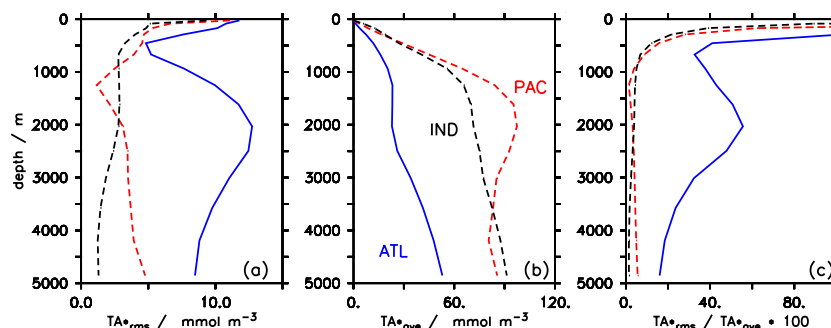
Figure 8. Basin-average vertical profiles of TA* RMSE **(a)**, TA* **(b)** and the percent ratio of the two **(c)**. Blue solid: Atlantic Ocean. Red dashed: Pacific Ocean. Black dashed: Indian Ocean.

Table 3. Volume-weighted RMSEs for TA^0 and TA* estimates based on seasonally unbiased TA^0 algorithm (all months) and winter- and summer-biased algorithms respectively. Column "surface" refers to the skill of the respective algorithm to reproduce the surface (upper 100 m) alkalinity of the model. Column TA^0 gives RMSEs of subsurface preformed TA as compared with TA^0 from the explicit tracer. Column TA* gives the RMSE of computed TA* compared with TA* from the explicit tracer. Global algorithms are also evaluated concerning their skills on regional scales.

Algorithm	Surface	Global		Atlantic Ocean		Pacific Ocean		Indian Ocean	
		TA^0	TA*	TA^0	TA*	TA^0	TA*	TA^0	TA*
Global									
All months	9.6	6.5	5.9	10.2	10.4	4.3	2.8	4.4	3.8
Winter data	9.7	5.2	5.2	9.0	9.0	2.8	3.0	2.6	2.3
Summer data	9.3	8.2	7.3	12.3	12.2	6.0	3.9	6.4	5.7
Atlantic									
All months	9.8			10.3	10.1				
Winter data	9.7			9.3	9.2				
Summer data	9.3			11.2	11.1				
Pacific									
All months	9.2					3.1	3.5		
Winter data	9.2					3.0	4.6		
Summer data	9.0					4.1	3.0		
Indic									
All months	5.9							3.2	2.7
Winter data	6.2							2.2	2.0
Summer data	5.4							5.1	4.4

minerals of CaCO₃, calcite and aragonite, respectively, has sometimes erroneously been interpreted to indicate shallow CaCO₃ dissolution – see Friis (2006) and Friis et al. (2007) for a discussion. Here we show that, in addition, TA* in these waters usually cannot be determined accurately due to uncertainties in the TA^0 estimate.

6 Application of the TA* approach to GLODAP and three OCMIP5 models

Finally, we apply the TA* approach to an observation-based data product and to the output from three different models available at the Ocean Carbon Cycle Model Intercomparison Project data server (http://ocmip5.ipsl.fr; accessed April 2012). Note that this is not the output from the CMIP5 exercise, e.g. for MPI-ESM it is from C4MIP. As for the observations, we combine the GLODAP gridded data set of TA (Key et al., 2004) with T, S, PO₄ and O₂ from the annual climatology of the World Ocean Atlas 2009 (e.g. Antonov
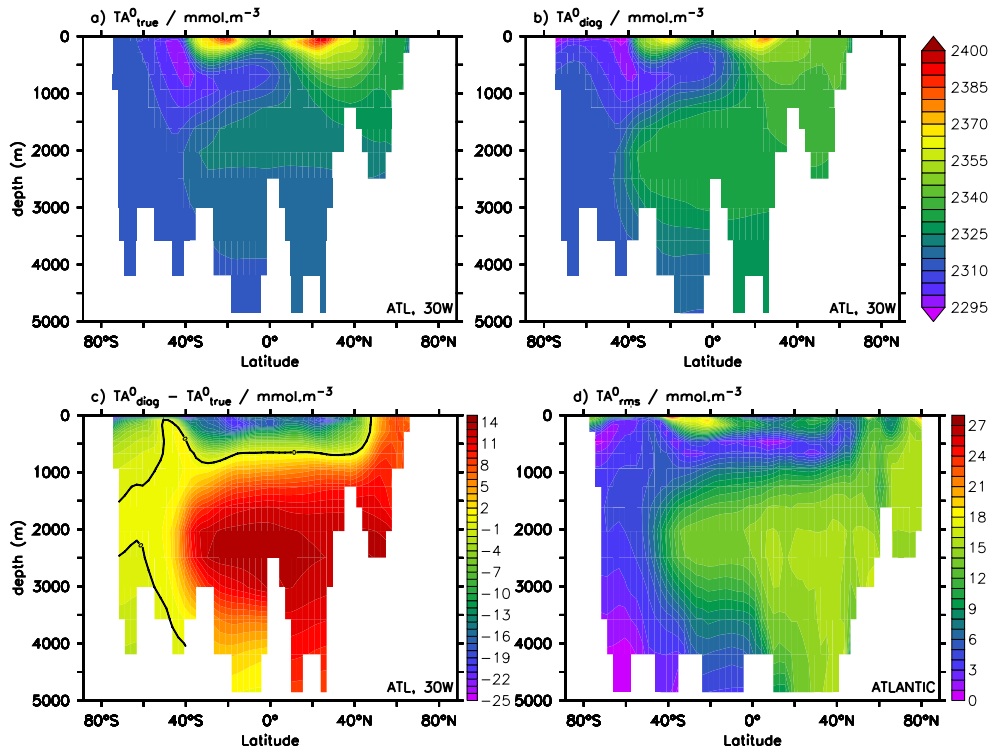
Figure 9. TA^0 distribution in the Atlantic Ocean from explicit tracer **(a)** and computed from winter biased surface sampling **(b)**. Panel **(c)** shows the anomaly between the two and panel **(d)** the basin average RMSE of TA^0.
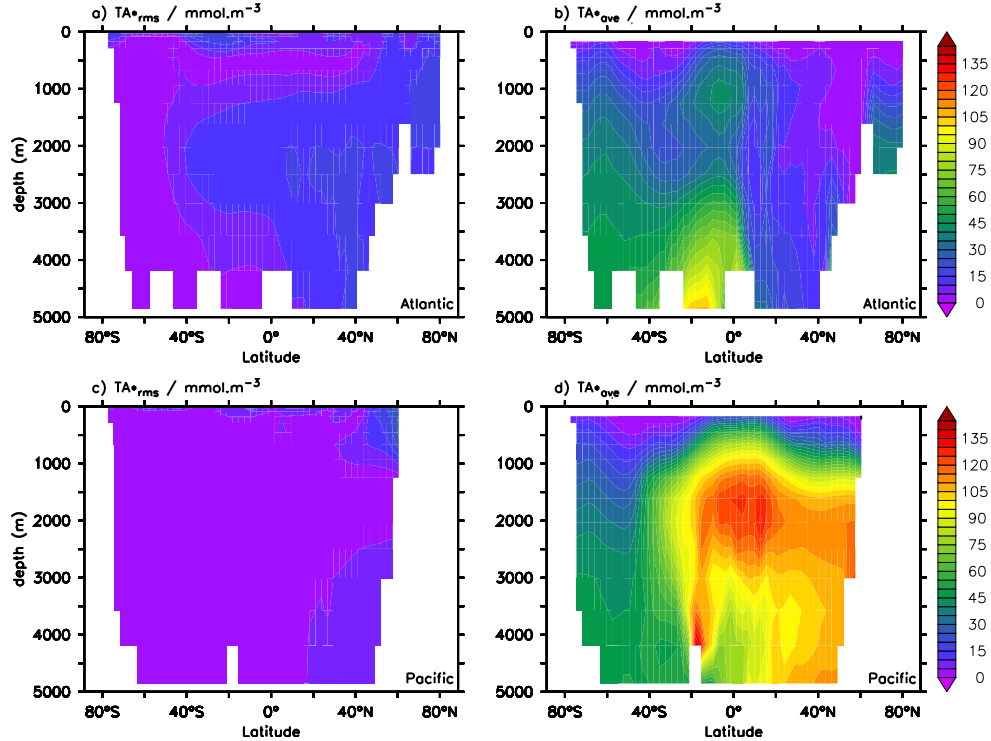

Figure 10. Basin averages of tracer-based TA* **(b, d)** and its RMSE (computed TA* vs. tracer TA*) from the Atlantic Ocean **(a)** and the Pacific Ocean **(c)**.
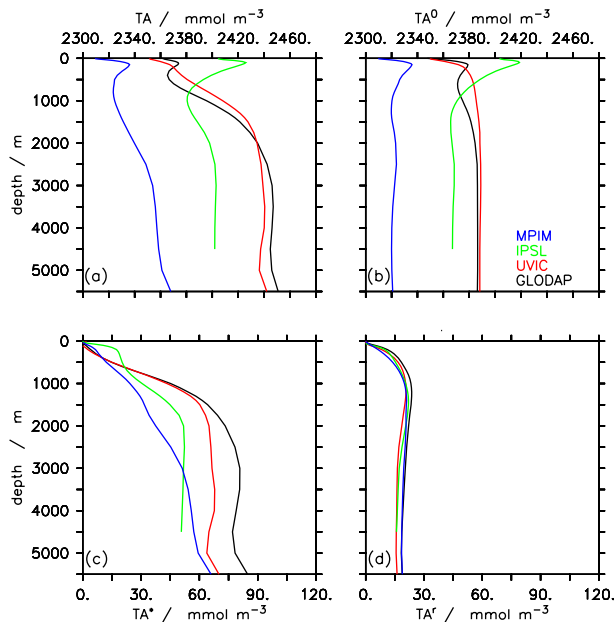
Figure 11. Global mean profiles of **(a)** TA, **(b)** TA^0, **(c)** TA* and **(d)** TA^r in the GLODAP data set and in three different models. Properties in **(b–d)** are diagnosed according to the methods described in Sect. 3. For each of the data sets a specific TA^0 algorithm was derived from annual mean data (models) or the annual composite GLODAP data, respectively (see text for details and insert for colour code of the models and data used).

et al., 2009). As for the models, we use output prepared for the control runs. Specifically, we use the first available annual time slice of either the CTL or HIST runs, representing the end of the respective model spin-up. We use output of the IFM/UVIC2-8 (Oschlies et al., 2008; http://ocmip5.ipsl.fr/models_description/ifm_uvic2-8.html), MPI-ESM with the marine carbon cycle component HAMOCC (Maier-Reimer et al., 2005; see also http://ocmip5.ipsl.fr/models_description/mpi-m_cosmos.html) and IPSL/IPSL-CM4 (Aumont and Bopp, 2006; see also http://ocmip5.ipsl.fr/models_description/ipsl_ipsl-cm4.html) models. It is beyond the scope of this paper to provide a full evaluation or model intercomparison of the three models. Instead we focus on a comparison of global mean profiles of TA, TA^0, TA^r and TA* from the three models and the observations with the only objective to illustrate the advantage of explicitly accounting for preformed alkalinity in a data-based model evaluation.

The global mean profile of alkalinity in the observations is characterized by an absolute minimum at the surface, a shallow maximum at about 100 to 200 m, a subsurface minimum at about 500 m, and a broad maximum between 3000 m and the bottom (Fig. 11a). The three models reproduce this structure to different degrees. The UVIC2-8 tracks the overall vertical gradient well while not reproducing the small-scale subsurface structures. The MPI-ESM tracks the vertical structure well, albeit with a too small overall vertical gradient, but

has a clear negative offset of about 80 mmol m^{-3}. This offset is due to losses to the sediment during the model spin-up. The IPSL-CM4 shows too high a TA in the upper 1000 m and too low a TA in the deep ocean by up to 40 mmol m^{-3} each. Subdividing TA into its components (TA^0, TA* and TA^r) indicates that much of the misfits or fits between the global mean profiles of the individual models and the data are due to differences in preformed alkalinity (Fig. 11b). This is the case for the negative offset of the MPI-ESM model, the wrong surface-to-deep gradient in IPSL-CM4, as well as the good agreement between UVIC2-8 and GLODAP concerning the surface-to-deep gradient and the overall shape of the vertical profiles. The subsurface shallow maxima and minima in the observed TA global profile are due to preformed TA^0 only, and they are not related to biogeochemical modifications of alkalinity. TA^r (Fig. 11d) as diagnosed from AOU global mean profiles shows small differences between models and data, in agreement with our expectations (see Sect. 5) that uncertainties in TA^r contribute little to uncertainties in the computation of TA*. The global mean profiles of TA* (Fig. 11c) suggest more agreement between models (and data) as might have been guessed from the global mean profiles of TA (Fig. 11a) alone. Yet, the globally integrated TA* inventory of IPSL-CM4 and MPI-ESM is about 25 % smaller than in both the GLODAP and the UVIC2-8 model. Also the distribution of TA* with respect to CaCO$_3$ saturation states varies considerably between models and observations (Table 4). In IPSL-CM4 and MPI-ESM, the models which underestimate global CaCO$_3$ dissolution, about two-thirds of the integrated TA* is found in waters where Ω_{CA}, the degree of saturation with respect to calcite is less than 1, while much smaller fractions are observed in waters with higher saturation. In GLODAP data the former fraction is about 55 % while the UVIC model has only 43 % of integrated TA* in undersaturated water. A large fraction of TA* in undersaturated water is in agreement with expectations from dissolution chemistry (e.g. Morse and Arvidson, 2002) and observations from the ocean where undersaturated waters in the North Pacific show the largest TA* (Feely et al., 2002). Overall, differences between observations and models both in the global integral of TA* and its distribution point to larger uncertainties in the CaCO$_3$ modules of coupled carbon cycle models than their organic tissue pump modules: on a global scale the time-accumulated imprint of organic matter remineralization on the oxygen distribution as measured by the AOU of several state-of-the-art models agreed within ± 10 % with observed AOU (Duteil et al., 2013; see also Fig. 11d).

The metric TA* allows us to compare the patterns of the imprint of CaCO$_3$ dissolution between models and the ocean. Hence, it may be used to identify the model which fits observations best. In the example of the three models compared it is the UVIC model which shows the most appropriate global mean profile of TA* (Fig. 11) and also the best fit of TA* patterns relative to CaCO$_3$ saturation (Table 4). The latter, in particular, is an interesting and surprising result, as the

Table 4. Global TA* inventories (Pmol C) and its fractions with respect to the CaCO$_3$ saturation states.

Model	Global TA* inventory (P mol C)	OmegaCa < 1 (%)	OmegaCa ≥ 1 and OmegaAR < 1 (%)	OmegaAr ≥ 1 (%)
GLODAP	38.9	55.3	41.3	3.4
IFM-UVIC28	40.0	43.0	49.1	7.9
IPSL-CM4	29.3	71.7	13.7	14.6
MPI-ESM	28.7	67.8	21.7	10.5

GLODAP is not defined north of 65° N. Model inventories and fractions are computed using the ocean volumes of the given model and the omega distribution in the respective models.

UVIC model applies the least mechanistic formulation of CaCO$_3$ dissolution of the three models. Both in the IPSL-CM4 and the MPI-ESM models, CaCO$_3$ dissolves depending on CaCO$_3$ undersaturation (Maier-Reimer et al., 2005; Aumont and Bopp, 2006), known as the dominant factor of CaCO$_3$ dissolution (Morse and Arvidson, 2002). The UVIC (Oschlies et al., 2008) instead applies an exponential decay function which dissolves CaCO$_3$ independent of the saturation state. To improve a model's mechanisms of CaCO$_3$ dissolution obviously does not (necessarily) improve its performance relative to an evaluation metric. The reasons for this are manifold. For any time-integrated property (like TA* or AOU) the age structure of the model is particularly relevant. Models with more sluggish deep water circulation will tend to show elevated ages (time since last contact with the atmosphere). With more time to accumulate the imprint of CaCO$_3$ dissolution or organic matter decay such models will also be characterized by higher TA* or AOU, in particular in the deep ocean. For this reason an analysis of the model age structure using suitable tracers (Koeve et al., 2014) is a fundamental element of model evaluation. Also, the absolute amount and horizontal patterns of CaCO$_3$ production affect the distribution of TA*. This can well be compared between models, but like other biogeochemical rates is not well constrained in the real ocean. Considering CaCO$_3$ dissolution in models with saturation-dependent dissolution formulations (e.g. IPSL-CM4, MPI-ESM), production patterns of organic matter together with the age structure control the patterns of AOU and thereby of respiratory carbon. This is a major determinant of CaCO$_3$ undersaturation in the deep ocean. Hence, in these models organic-matter-related processes have a significant impact on TA*. Also, the representation of CaCO$_3$ dissolution or burial in sediments (Dunne et al., 2012) may be of importance. Both the IPSL-CM4 and the MPI-ESM model contain a simple sediment module while the UVIC does not. The focus of this study is the assessment of the TA* method and not the evaluation of individual models which requires to disentangle the interactions of the different drivers of the TA* distribution. We leave this to a follow-up paper which will apply the TA* method in the framework of CMIP5 model analysis.

7 Conclusions

In this study we tested the applicability of the TA* approach (Feely et al., 2002) to quantify the time-integrated and advected signal of CaCO$_3$ dissolution in models and observations by means of an ocean carbon cycle model augmented with idealized tracers of CaCO$_3$ dissolution. The method of computing TA* according to the scheme described in Sect. 3 is found to reproduce tracer-based TA* in our model experiment robustly in most of the global ocean. It is mainly in the Atlantic Ocean, but also in the upper 500 to 1000 m of the Pacific and Indian oceans, respectively, where computed TA* has elevated uncertainty, which makes it unsuited to derive cumulative CaCO$_3$ dissolution in these waters. Since most of this uncertainty arises from the uncertainty of the TA^0 estimate, alternative approaches to derive isopycnal-specific preformed alkalinity, e.g. from methods of isopycnal analysis (e.g. Körtzinger et al., 2001), in combination with techniques to estimate water mass fractions in the ocean interior (e.g. Karstensen and Tomczak, 1998; Khatiwala et al., 2012) may be worth testing for regional applications. When comparing computed TA* from observational data and model output an additional source of uncertainty may arise from the TA^r term of Eq. (1). Usually this term is computed starting from AOU as a measure of organic matter remineralization. However, as shown by Ito et al. (2004), AOU overestimates true oxygen utilization by 20–25 %. Hence TA^r computed from AOU is probably also overestimated by this percentage if we ignore the additional uncertainty related to the assumption of constant elemental ratios (Koeve, 2004, 2006). Since the difference between AOU and true oxygen utilization varied considerable between models (Duteil et al., 2013), we propose to use a recently developed metric, the Evaluated Oxygen Utilization (EOU) (Duteil et al., 2013) instead of AOU also for the computation of TA^r.

As demonstrated from observations and model experiments, TA includes a large (and generally dominant) fraction of preformed alkalinity, closely associated with the salinity field and hence the physics of the ocean. Approaches in which alkalinity is normalized to salinity, like PALK or TA^{H06} were, however, shown to produce "artificial" patterns in the interior of the ocean which are often not related to local biogeochemical processes. These TA derivatives do not fully remove the salinity association of patterns. In addition TA derivatives can be biased by the imprint of remote biogeochemical processes. For example, Southern Ocean upwelling and re-injection of water with an imprint from CaCO$_3$ dissolution in the North Pacific can give the false impression of CaCO$_3$ dissolution taking place in the South Atlantic. We conclude that data–model comparisons based on TA or salinity-normalized alkalinity alone cannot evaluate the CaCO$_3$ model independent of any possible deficiencies in the physical model.

In the TA* approach the conservative component of alkalinity is treated explicitly and separated from the components related to biogeochemical processes. This turned out to be successful in much of the ocean in our method-assessment model experiment. Applying the TA* approach to model output from three state-of-the-art ocean carbon cycle models we demonstrated the advantage of explicitly taking preformed alkalinity into account when comparing a range of CaCO$_3$ cycle models with observations. The comparison of these (albeit few) models with observations points to larger uncertainties in the CaCO$_3$ modules of coupled carbon cycle models than in the representation of the organic tissue pump in the same models.

Finally, we propose to use the TA* approach for the data-based evaluation of models of the oceanic CaCO$_3$ cycle. Similar to a proposal made for the organic tissue pump by Najjar et al. (2007), we suggest to implement idealized tracers of either TA^0 or TA* in ocean biogeochemical models in order to ease model intercomparison, but also to test whether the results from this model study which applied a rather pragmatic parametrization of CaCO$_3$ dissolution are applicable to a wider range of ocean models using different CaCO$_3$ cycle parametrizations.

References

Anderson, L. A. and Sarmiento, J. L.: Redfield ratios of remineralization determined by nutrient data analysis, Global Biogeochem. Cy., 8, 65–80, 1994.

Anonymous: Interactive comment on "Evaluating CaCO$_3$-cycle modules in coupled global biogeochemical ocean models" by W. Koeve et al., Geosci. Model Dev. Discuss., 6, 6117-6155, doi:10.5194/gmdd-6-6117-2013, 2013.

Antonov, J. I., Seidov, D., Boyer, T. P., Locarnini, R. A., Mishonov, A. V., Garcia, H. E., Baranova, O. K., Zweng, M. M., and Johnson, D. R.: World Ocean Atlas 2009, vol. 2: Salinity, NOAA Atlas NESDIS 69, US Government Printing Office, Washington, DC, 184 pp., 2010.

Aumont, O. and Bopp, L.: Globalizing results from ocean in situ iron fertilization studies, Global Biogeochem. Cy., 20, GB2017, doi:10.1029/2005GB002591, 2006.

Berelson, W. M., Balch, W. M., Najjar, R., Feely, R. A., Sabine, C., and Lee, K.: Relating estimates of CaCO$_3$ production, export, and dissolution in the water column to measurements of CaCO$_3$ rain into sediment traps and dissolution on the sea floor: a revised global carbonate budget, Global Biogeochem. Cy., 21, GB1024, doi:10.1029/2006GB002803, 2007.

Broecker, W. S.: "NO", a conservative water-mass tracer, Earth Planet. Sc. Lett., 23, 100–107, 1974.

Cai, W.-J., Hu, X., and Juang, W.-J., Jiang, L. Q., Wang, Y., Peng, T.-H., and Zhang, X.: Alkalinity distribution in the western North Atlantic Ocean margins, J. Geophys. Res., 115, C08014, doi:10.1029/2009JC005482, 2010.

Chen, G.-T. and Millero, F. J.: Gradual increase of oceanic CO$_2$, Nature, 277, p. 205, 1979.

Chung, S.-N., Lee, K., Feely, R. A., Sabine, C. L., Millero, F. J., Wanninkhof, R., Bullister, J. L., Key, R. M., and Peng, T.-H.: Calcium carbonate budget in the Atlantic Ocean based on water column inorganic carbon chemistry, Global Biogeochem. Cy., 17, 1093, doi:10.1029/2002GB002001, 2003.

Doney, S. C., Lindsay, K., Caldeira, K., Campin, J.-M., Drange, H., Dutay, J.-C., Follows, M., Gao, Y., Gnanadesikan, A., Gruber, N., Ishida, A., Joos, F., Madec, G., Maier-Reimer, E., Marschall, J. C., Matear, R. J., Monfray, P., Mouchet, A., Najjar, R., Orr, J. C., Plattner, G.-K., Sarmiento, J., Schlitzer, R., Slater, R., Totterdell, I. J., Weirig, M.-F., Yamanaka, Y., and Yool, A.: Evaluating global ocean carbon models: the importance of realistic physics, Global Biogeochem. Cy., 18, GB3017, doi:10.1029/2003GB002150, 2004.

Dunne, J. P., Hales, B., and Toggweiler, J. R.: Global calcite cycling constrained by sediment preservation controls, Global Biogeochem. Cy., 26, GB3023, doi:10.1029/2010GB003935, 2012.

Duteil, O., Koeve, W., Oschlies, A., Aumont, O., Bianchi, D., Bopp, L., Galbraith, E., Matear, R., Moore, J. K., Sarmiento, J. L., and Segschneider, J.: Preformed and regenerated phosphate in ocean general circulation models:

can right total concentrations be wrong?, Biogeosciences, 9, 1797–1807, doi:10.5194/bg-9-1797-2012, 2012.

Duteil, O., Koeve, W., Oschlies, A., Bianchi, D., Kriest, I., Galbraith, E., and Matear, R.: A new estimate of ocean oxygen utilization points to a reduced rate of respiration in the ocean interior, Biogeosciences, 10, 7723–7738, doi:10.5194/bg-10-7723-7738, 2013.

Feely, R. A., Sabine, C. L., Lee, K., Millero, F. J., Lamb, M. F., Greeley, D., Bullister, J. L., Key, R. M., Peng, T.-H., Kozyr, A., Ono, T., and Wong, C. S.: In situ calcium carbonate dissolution in the Pacific Ocean, Global Biogeochem. Cy., 16, 1144, doi:10.1029/2002GB001866, 2002.

Friis, K.: A review of marine anthropogenic CO₂ definitions: introducing a thermodynamic appraoch based on observations, Tellus B, 58, 2–15, 2006.

Friis, K., Körtzinger, A., and Wallace, D. W. R.: A concept study on the use and misuse of salinity-normalised alkalinity data, Geophys. Res. Lett., 30, 1085, doi:10.1029/2002GL015898, 2003.

Friis, K., Najjar, R. G., Follows, M. J., Dutkiewicz, S., Körtzinger, A., and Johnson, K. M.: Dissolution of calcium carbonate: observations and model results in the subpolar North Atlantic, Biogeosciences, 4, 205–213, doi:10.5194/bg-4-205-2007, 2007.

Gehlen, M., Gangstø, R., Schneider, B., Bopp, L., Aumont, O., and Ethe, C.: The fate of pelagic CaCO₃ production in a high CO₂ ocean: a model study, Biogeosciences, 4, 505–519, doi:10.5194/bg-4-505-2007, 2007.

Howard, M. T., Winguth, A. M. E., Klaas, C., and Maier-Reimer, E.: Sensitivity of ocean carbon tracer distributions to particulate organic flux parameterizations, Global Biogeochem. Cy., 20, GB2011, doi:10.1029/2005GB002499, 2006.

Ilyina, T., Zeebe, R. E., Maier-Reimer, E., and Heinze, C.: Early detection of ocean acidification effects on marine calcification, Global Biogeochem. Cy., 23, GB1008, doi:10.1029/2008GB003278, 2009.

Ito, T., Follows, M. J., and Boyle, E. A.: Is AOU a good measure of respiration in the ocean?, Geophys. Res. Lett., 31, L17305, doi:10.1029/2004GL020900, 2004.

Kanamori, S. and Ikegami, H.: Calcium–alkalinity relationship in the North Pacific, J. Oceanogr. Soc. Jpn., 38, 57–62, 1982.

Karstensen, J. and Tomczak, M.: Age determination of mixed water masses using CFC and oxygen data, J. Geophys. Res., 103, 18599–18609, 1998.

Key, R. M., Kozyr, A., Sabine, C. L., Lee, K., Wanninkhof, R., Bullister, J. L., Feely, R. A., Millero, F. J., Mordy, C., and Peng, T.-H.: A global ocean carbon climatology: results from Global Data Analysis Project (GLODAP), Global Biogeochem. Cy., 18, GB4031, doi:10.1029/2004GB002247, 2004.

Khatiwala, S.: A computational framework for simulation of biogeochemical tracers in the ocean, Global Biogeochem. Cy., 21, GB3001, doi:10.1029/2007GB002923, 2007.

Khatiwala, S., Visbeck, M., and Cane, M. A.: Accelerated simulation of passive tracers in ocean circulation models, Ocean Model., 9, 51–69, 2005.

Khatiwala, S., Primeau, F., and Holzer, M.: Ventilation of the deep ocean constrained with tracer observations and implications for radiocarbon estimates of ideal mean age, Earth Planet. Sc. Lett., 325, 116–125, 2012.

Koeve, W.: Spring bloom carbon to nitrogen ratio of net community production in the temperate N. Atlantic, Deep-Sea Res. Pt. I, 51, 1579–1600, 2004.

Koeve, W.: Stoichiometry of the biological pump in the North Atlantic – constraints from climatological data, Global Biogeochem. Cy., GB3018, doi:10.1029/2004GB002407, 2006.

Koeve, W., Wagner, H., Kähler, P., and Oschlies, A.: 14C-ages in global ocean circulation models, Geosci. Model Dev. Discuss., submitted, 2014.

Körtzinger, A., Koeve, W., Kähler, P., and Mintrop, L.: C : N ratios in the mixed layer during the productive season in the northeast Atlantic ocean, Deep-Sea Res. Pt. I, 48, 661–688, 2001.

Kriest, I., Khatiwala, S., and Oschlies, A.: Towards and assessment of simple global marine biogeochemical models of different complexity, Prog. Oceanogr., 86, 337–360, 2010.

Kriest, I., Oschlies, A., and Khatiwala, S.: Sensitivity analysis of simple global marine biogeochemical models, Global Biogeochem. Cy, 26, GB2029, doi:10.1029/2011GB004072, 2012.

Marshall, J. and Speer, K.: Closure of the meridional overturning circulation through Southern Ocean upwelling, Nat. Geosci., 5, 171–180, 2012.

Marshall, J., Adcroft, A., Hill, C., Perelman, L., and Heisey, C.: A finite-volume, incompressible navier-stokes model for studies of the ocean on parallel computers, J. Geophys. Res., 102, 5733–5752, 1997.

Martin, J. H., Knauer, G. A., Karl, D. M., and Broenkow, W. W.: VERTEX: carbon cycling in the northeast Pacific, Deep-Sea Res., 34, 267–285, 1987.

Matsumoto, K. and Gruber, N.: How accurate is the estimation of anthropogenic carbon in the ocean? An evaluation of the ΔC* method, Global Biogeochem. Cy., 19, GB3014, doi:10.1029/2004GB002397, 2005.

Maier-Reimer, E., Kriest, I., Segschneider, J., and Wetzel, P.: The Hamburg ocean carbon cycle model HAMOCC5.1. Technical description, Release 1.1. Berichte zur Erdsystemforschung, 14/2005, Max-Planck-Institut für Meteorologie, 2005.

Morse, J. W. and Arvidson, R. S.: The dissolution kinetics of major sedimentary carbonate minerals, Earth-Sci. Rev., 58, 51-84, 2002.

Najjar, R. G., Jin, X., Louanchi, F., Aumont, O., Caldeira, K., Doney, C. S., Dutay, J.-C., Follows, M., Gruber, N., Joos, F., Lindsay, K., Maier-Reimer, E., Matear, R. J., Matsumoto, K., Monfray, P., Mouchet, A., Orr, J. C., Plattner, G.-K., Sarmiento, J. L., Schlitzer, R., Slater, R. D., Wierig, M.-F., Yamanaka, Y., and Yool, A.: Impact of circulation on export production, dissolved organic matter, and dissolved oxygen in the ocean: results from phase II of the Ocean Carbon-cycle Model Intercomparison Project (OCMIP-2), Global Biogeochem. Cy., 21, GB3007, doi:10.1029/2006GB002857, 2007.

Omta, A. W., Goodwin, P., and Follow, M. J.: Multiple regimes of air-sea carbon partitioning identified from constant-alkalinity buffer factors, Global Biogeochem. Cy., 24, GB3008, doi:10.1029/2009GB003726, 2010.

Omta, A. W., Dutkiewicz, S., and Follows, M. J.: Dependence of the ocean-atmosphere partitioning of carbon on temperature and alkalinity, Global Biogeochem. Cy., 25, GB1003, doi:10.1029/2010GB003839, 2011.

Oschlies, A., Schulz, K. G., Riebesell, U., and Schmittner, A.: Simulated 21st centuryís increase in oceanic suboxia by CO₂-

enhanced biotic carbon export, Global Biogeochem. Cy., 22, GB4008, doi:10.1029/2007GB003147, 2008.

Pytkowicz, R. M.: On the apparent oxygen utilization and the preformed phosphate in the oceans, Limnol. Oceanogr., 16, 39–42, 1971.

Redfield, A. C., Ketchum, B. H., and Richards, F. A.: The influence of organisms on the composition of sea-water, in: The Sea, vol. 2, edited by: Hill, M. N., Whiley-Intersciences, New York, 26–77, 1963.

Ridgwell, A., Zondervan, I., Hargreaves, J. C., Bijma, J., and Lenton, T. M.: Assessing the potential long-term increase of oceanic fossil fuel CO_2 uptake due to CO_2-calcification feedback, Biogeosciences, 4, 481–492, doi:10.5194/bg-4-481-2007, 2007.

Robbins, P. E.: Oceanic carbon transport carried by freshwater divergence: are salinity normalizations useful?, J. Geophys. Res., 106, 30939–30946, 2001.

Sabine, C. L., Key, R. M., Feely, R. A., and Greeley, D.: Inorganic carbon in the Indian Ocean: distribution and dissolution processes, Global Biogeochem. Cy., 16, 1067, doi:10.1029/2002GB001869, 2002.

Sabine, C. L., Feely, R. A., Gruber, N., Key, R. M., Lee, K., Bullister, J. L., Wanninkhof, R., Wong, C. S., Wallace, D. W. R., Tilbrook, B., Millero, F. J., Peng., T.-H., Kozyr, A., Ono, T., and Rios, A. F.: The oceanic sink for anthropogenic CO_2, Science, 305, 367–371, 2004.

Sarmiento, J. L., Dunne, J., Gnanadesikan, A., Key, R. M., Matsumoto, K., and Slater, R.: A new estimate of the CaCO₃ to organic carbon export ratio, Global Biogeochem. Cy., 16, GB1107, doi:10.1029/2002GB001919, 2002.

Sarmiento, J. L. and Gruber, N.: Ocean Biogeochemical Dynamics, Princeton University Press, Princeton and Oxford, 503 pp., 2006

Schmittner, A., Oschlies, A., Giraud, X., Eby, M., and Simmons, H. L.: A global model of the marine ecosystem for long-term simulations: sensitivity to ocean mixing, buoyancy forcing, particle sinking, and dissolved organic matter cycling, Global Biogeochem. Cy., 19, GB3004, doi:10.1029/2004GB002283, 2005.

Séférian, R., Bopp, L., Gehlen, M., Orr, J. C., Ethé, C., Cadule, P., Aumont, O., Mélia, D. S. Y., Voldoire, A., and Madec, G.: Skill assessment of three earth system models with common marine biogeochemistry, Clim. Dynam., 40, 2549–2573, doi:10.1007/s00382-012-1362-8, 2013.

Schneider, B., Bopp, L., and Gehlen, M.: Assessing the sensitivity of modeled air-sea CO_2 exchange to the remineralization depth of particulate organic and inorganic carbon, Global Biogeochem. Cy., 22, GB3021, doi:10.1029/2007GB003100, 2008.

Wolf-Gladrow, D. A., Zeebe, R. E., Klaas, C., Körtzinger, A., and Dickson, A. G.: Total alkalinity: the explicit conservative expression and its application to biogeochemical processes, Mar. Chem., 106, 287–300, 2007.